Surface Plasmon–Enhanced Luminescence of Silicon Quantum Dots in Gold Nanoparticle Composites

ARTICLE *in* THE JOURNAL OF PHYSICAL CHEMISTRY C · OCTOBER 2015

Impact Factor: 4.77 · DOI: 10.1021/acs.jpcc.5b08105

4 AUTHORS:

Asuka Inoue

Kobe University

1 PUBLICATION **0** CITATIONS

SEE PROFILE

Minoru Fujii

Kobe University

336 PUBLICATIONS **6,526** CITATIONS

SEE PROFILE

Hiroshi Sugimoto

Kobe University

18 PUBLICATIONS **116** CITATIONS

SEE PROFILE

Kenji Imakita

Kobe University

89 PUBLICATIONS **593** CITATIONS

SEE PROFILE

THE JOURNAL OF PHYSICAL CHEMISTRY C

Article

pubs.acs.org/JPCC

Surface Plasmon-Enhanced Luminescence of Silicon Quantum Dots in Gold Nanoparticle Composites

Asuka Inoue, Minoru Fujii,* Hiroshi Sugimoto, and Kenji Imakita

Department of Electrical and Electronic Engineering, Graduate School of Engineering, Kobe University, Rokkodai, Nada, Kobe 657-8501, Japan

Supporting Information

ABSTRACT: A composite nanoparticle (NP) consisting of a gold nanoparticle (Au-NP) core and a thick shell of silicon quantum dot (Si-QD) agglomerates was developed. In the composite NPs with an optimized amount of Si-QDs per a Au-NP, photoluminescence from Si-QDs was enhanced, when it was excited in the wavelength range of the localized surface plasmon resonances (LSPRs) of Au-NPs. The experimental results could be well-explained by a simple model consisting of a spherical Au-NP and a spherical shell made from Si-QD aggregates. It was found that the enhancement is due to increased excitation efficiency of Si-QDs via the LSPR of Au-NPs.

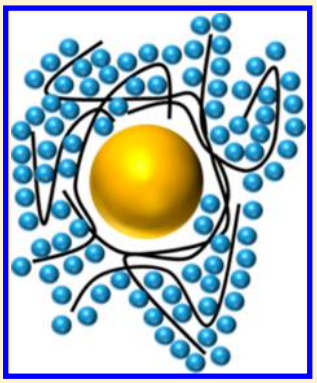

INTRODUCTION

Semiconductor quantum dots (QDs) have many attractive features, such as wide tunability of the luminescence energy, high chemical stability in aqueous media, and high photostability during long-term illumination, and have been expected to take the place of organic dyes for biomedical labeling and imaging applications.[1−5] A concern of the biomedical applications is hazardous heavy metal elements in commercially available Cd and Pb chalcogenide QDs. An alternative candidate to have potential to replace them is Si-QDs, which have high biocompatibility and biodegradability.[6−11] Intensive research has been done to develop water-dispersible and highly luminescent Si-QDs for biological applications.[12] Park et al. reported in vivo imaging in dextran-coated porous Si nanoparticles.[13] They also demonstrated efficient degradation in vivo. Erogbogbo et al. developed micelle-encapusulated Si-QDs exhibiting fluorescence in Panc-1 cells in vitro.[8] He et al. reported in vitro imaging by using polymeric nanospheres where Si-QDs are incorporated into a poly(acrylic acid) matrix.[14]

For biological applications of QDs, the luminescence wavelength is preferably within the transparent window of tissue (700−900 nm).[15] Tuning the luminescence wavelength in this range can be achieved easily in Si-QDs.[16,17] Luminescence of Si-QDs can be excited efficiently by blue or ultraviolet (UV) light, although the penetration depth in tissue is sacrificed. Furthermore, autofluorescence from tissue under high-energy photon excitation severely degrades the signal-to-background ratio. These problems can be avoided by using low-energy photons for excitation. However, the excitation efficiency of Si-QDs in the long wavelength range is extremely small due to the indirect nature of the band structure below ∼3.4 eV. Therefore, enhancement of the excitation cross-section of Si-QDs in the long wavelength range is an urgent issue to make them practical in biological applications.

A promising approach to achieve enhancement is utilizing enhanced electric fields accompanied by the excitation of surface plasmon resonances of metal nanostructures. Enhancement of the luminescence intensity and the decay rate of Si-QDs attached on a variety of plasmonic substrates has been reported.[18−22] Furthermore, different types of nanocomposites, which consist of Si-QDs and metal nanostructures, have been developed. Erogbogbo et al. produced a structure consisting of a core of Si-QD agglomerates and a Au shell.[23] Harun et al. encapsulated Si-QDs and Au-NPs in polymer nanoparticles and observed strong enhancement of the luminescence intensity.[24] Sugimoto et al. studied the effect of a Au nanorod on the luminescence properties of Si-QDs, when they are attached on the surface of a nanorod.[25] These nanocomposites are an independent functional system and can be used in a variety of applications, including imaging and sensing. However, research on metal/Si-QD nanocomposites is still very limited, and development of practically useful nanocomposites is highly demanded.

In this work, we develop a core−shell-type Si-QD-based nanocomposite consisting of a Au nanoparticle (NP) core and a thick shell of Si-QD agglomerates. We demonstrate that nanocomposite formation results in the enhancement of the photoluminescence (PL) from Si-QDs in the near-infrared range, when the excitation wavelength is around the resonance

Received: August 20, 2015
Revised: October 9, 2015
Published: October 13, 2015

DOI: 10.1021/acs.jpcc.5b08105
J. Phys. Chem. C 2015, 119, 25108−25113

wavelength of the localized surface plasmon resonance (LSPR) of Au-NPs. We also show that the enhancement factor depends on the average number of Si-QDs per a Au-NP, and optimization of the number is necessary to achieve the enhancement. A simple model structure consisting of a spherical Au-NP and a spherical shell made of Si-QD aggregates is considered, and the excitation wavelength dependence of the PL enhancement factor is calculated for different shell thicknesses.

EXPERIMENTAL METHOD

We employ B- and P-codoped Si-QDs developed in our group for the formation of nanocomposites.[16,26−28] The codoped Si-QD has a high B and P concentration shell, and the surface is negatively charged (ζ-potential ∼−30 mV).[29] The surface potential prevents agglomeration of Si-QDs by the electrostatic repulsion, and thus, they are dispersed in polar solvents without surface functionalization processes. The high solution dispersibility is an important advantage for the formation of nanocomposites.

Codoped Si-QDs were prepared by the method described in our previous papers.[16,26−28] Si-rich borophosphosilicate glass (BPSG) films were deposited by cosputtering Si, SiO_2, B_2O_3, and P_2O_5 in an rf-sputtering apparatus. The films were peeled from a substrate and annealed at 1100−1200 °C in a N_2 gas atmosphere for 30 min. By annealing, B- and P-codoped Si-QDs are grown in BPSG matrixes. The average diameter of the Si-QDs is changed from 4 to 7 nm when the growth temperature is changed from 1100 to 1200 °C. The BPSG matrixes were then etched out by HF (46 wt %) solution, and isolated Si-QDs were extracted and dispersed in methanol. Figure 1a shows a methanol solution of codoped Si-QDs. The solution is very clear due to perfect dispersion of Si-QDs in methanol.

Figure 1b shows a schematic illustration of the preparation procedure of Au-NP/Si-QD composites. Negatively charged citrate-coated Au-NPs (50 nm in diameter) were purchased from BBI Solutions (EMGC 50). A 600 μL volume of the solution was added drop-per-drop under vigorous stirring in 600 μL of distilled water containing 3.8 mg of poly(allylamine hydrochloride) (PAH) previously sonicated in an ultrasonic bath for 20 min.[30] In this process, Au-NPs are covered by PAH and positively charged. Residual PAH was removed by centrifugation, and Au-NPs were redispersed in distilled water. Finally, the methanol solution of Si-QDs was added to Au-NPs dispersed in water to produce Au-NP/Si-QD composites.

The morphology and structure of the Au-NP/Si-QD composites were characterized by transmission electron microscopy (TEM) (JEM-2100F, JEOL). PL and PL excitation (PLE) spectra of the composite were obtained by using a spectrophotometer (Fluorolog-3, Horiba Jovin Yvon) equipped with a Xe lamp (450 W) and a double-grating monochromator as an excitation source. PL decay curves were obtained by using an image-intensified charge-coupled device (CCD). The excitation source was modulated 405 nm light from a laser diode.

RESULTS AND DISCUSSION

Figure 1c shows a TEM image of a Au-NP/Si-QD composite for Si-QDs grown at 1200 °C. A Au-NP about 50 nm in diameter is coated by Si-QDs. Figure 1d shows a high-resolution TEM image of a Si-QD. Lattice fringes corresponding to the {111} planes of Si can clearly be seen. The diameter of the Si-QD is about 7 nm. The irregular shape of the Au-NP/Si-QD composite in Figure 1c suggests that the mechanism of the composite formation is not the electrostatic attraction between positively charged Au-NPs and negatively charged Si-QDs. It seems that Si-QDs are arrested by PAH around a Au-NP as schematically shown in Figure 1b. The shapes of the composites are distributed in a wide range, and in some cases, a few Au-NPs are contained in a composite. TEM images of several different composites are shown in the Supporting Information (see Figures S1 and S2).

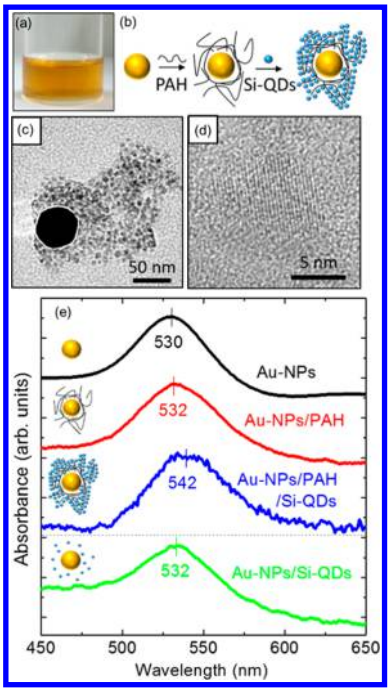

Figure 1. (a) Photograph of a methanol solution of Si-QDs. (b) Schematic illustration of the composite preparation procedure. (c) TEM image of a Au-NP/Si-QD composite. (d) High-resolution TEM image of a Si-QD in a composite. (e) Absorption spectra of solutions of Au-NPs (black), PAH-coated Au-NPs (red), and Au-NP/Si-QD composites (blue). The spectrum of a mixed solution of as-purchased Au-NPs and Si-QDs is also shown (green).

Figure 1e shows absorption spectra of Au-NPs at different steps of the composite formation process. As-purchased Au-NPs in distilled water have the LSPR peak at 530 nm. PAH coating results in a slight shift to longer wavelength due to the increase of the surrounding dielectric constant.[30] After the formation of the composite, the peak shifts to 542 nm. The large shift confirms that composites are formed in a majority of Au-NPs in the solution. It is noted that the shift is not observed when untreated Au-NPs are mixed with Si-QDs (bottom spectrum in Figure 1e). Therefore, PAH coating is a crucial step for the formation of the composite.

Figure 2a shows PL and PLE spectra of Si-QDs grown at 1100 °C in methanol excited at 532 nm together with the absorption spectrum of as-purchased Au-NPs. The detection wavelength for the PLE measurement is set to the PL peak (∼780 nm). The PLE spectrum shows that the excitation efficiency is very small above 500 nm, because of the indirect nature of the energy band structure. In Au-NP/Si-QD composites, the excitation efficiency is expected to be enhanced around the LSPR wavelength. To study the enhancement of the

DOI: 10.1021/acs.jpcc.5b08105
J. Phys. Chem. C 2015, 119, 25108−25113

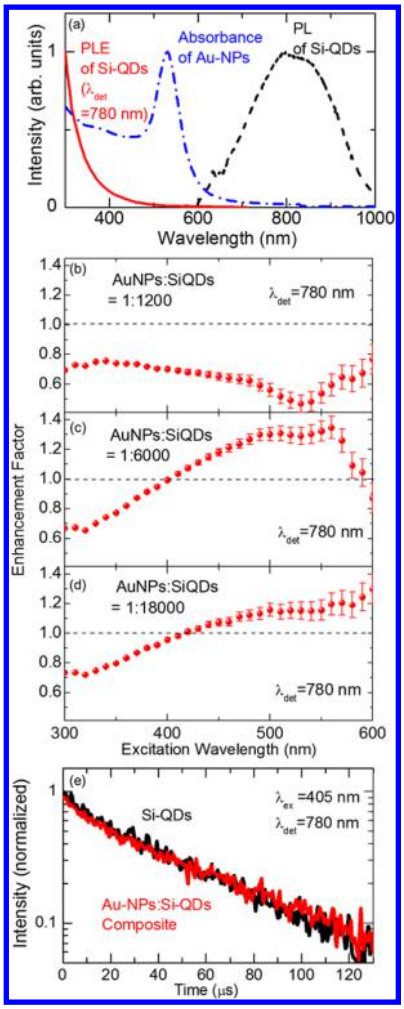

Figure 2. (a) PL spectrum excited at 532 nm (black) and PLE spectrum detected at 780 nm (red) of Si-QDs in solution. The absorption spectrum of Au-NPs in solution is also shown (black dashed line). (b–d) Enhancement factors of PLE spectra of Au-NP/Si-QD composites with different Au-NP:Si-QD number ratios: (b) 1:1200, (c) 1:6000, (d) 1:18000. The detection wavelength is 780 nm. (e) PL decay curves of Si-QDs (black) and Au-NP/Si-QD composites (red) in solutions. The excitation and detection wavelengths are 405 and 780 nm, respectively.

excitation efficiency by the formation of the composite, PLE spectra of solutions containing Au-NP/Si-QD composites are measured, and they are divided by that of a solution containing the same amount of Si-QDs (PLE enhancement factor). The results obtained for samples with different number ratios of Au-NPs and Si-QDs (Au-NPs:Si-QDs) are shown in Figure 2b–d. Note that Au-NPs:Si-QDs = 1:1200 means that nominally on average 1200 Si-QDs are attached on a Au-NP, although the number of Si-QDs is distributed in a wide range within a sample as can be seen in the Supporting Information (Figures S1 and S2). When Au-NPs:Si-QDs is 1:1200 (Figure 2b), the spectrum has a broad dip around 530 nm, which exactly coincides with the LSPR wavelength of Au-NPs. Therefore, in this preparation condition, composite formation deteriorates the excitation efficiency of Si-QDs. This is probably due to the fact that the number of Si-QDs is not large enough and Au-NPs not well-decorated with Si-QDs remain.

The situation is different when the amount of Si-QDs is increased (Au-NPs:Si-QDs = 1:6000) (Figure 2c). The PLE enhancement factor reaches a maximum of 1.3 around 530 nm. This is considered to be due to the enhancement of the excitation efficiency of Si-QDs by Au-NPs. When the amount of Si-QDs is further increased (Au-NPs:Si-QDs = 1:18000), the maximum enhancement factor decreases slightly (1.2-fold) (Figure 2d). This may be due to an increased thickness of the Si-QD shell and the resultant increase of the number of Si-QDs not receiving benefits of local field enhancements by Au-NPs. The shell-thickness dependence of the enhancement factor will be discussed later from the theoretical calculations.

In Figure 2e, the PL decay curves of Si-QDs and Au-NP/Si-QD composites in solutions are compared. The comparison of the PL spectra is shown in Supporting Information (Figure S3). Because of detuning of the LSPR peak from the PL peak, the PL spectral shapes and the decay rates are not affected by the formation of the composites. This confirms that the PL enhancement in Figure 2c,d is not due to the enhancement of the radiative decay rate or the quantum efficiency, but due to that of the excitation efficiency.

In Figure 2c,d, when the excitation wavelength is below 400 nm, the enhancement factor is smaller than 1. In this wavelength range, absorption by Au-NPs is not due to the LSPR but due to the interband transitions.[31] Therefore, excitation photons absorbed by Au-NPs do not contribute to the absorption enhancement of Si-QDs.

To understand the mechanism of the observed PL enhancement, we calculate the PL enhancement factor as a function of the wavelength. Since the composites have complicated shapes, an accurate estimation of the enhancement factor is not possible. However, an average enhancement factor of many composites in solution may be roughly estimated by assuming that the composites consist of a spherical Au-NP core and a spherical shell made from Si-QDs as schematically shown in Figure 3a. In the structure, we calculate the enhancement factor of the incident electric fields and the decay rates (Purcell factor) in the shell, and estimate the PL enhancement factor at different excitation wavelengths.

For the calculation, we have to know the effective dielectric function of the shell ($\varepsilon_{\mathrm{eff}}$). We employ the Bruggeman effective medium approximation, $f_{\mathrm{Si}}[(\varepsilon_{\mathrm{Si}} - \varepsilon_{\mathrm{eff}})/(\varepsilon_{\mathrm{Si}} + 2\varepsilon_{\mathrm{eff}})] + (1 - f_{\mathrm{Si}})[(\varepsilon_{\mathrm{H_2O}} - \varepsilon_{\mathrm{eff}})/(\varepsilon_{\mathrm{H_2O}} - 2\varepsilon_{\mathrm{eff}})] = 0$, where $\varepsilon_{\mathrm{Si}}$ and $\varepsilon_{\mathrm{H_2O}}$ are the dielectric functions of Si[32] and water ($\varepsilon_{\mathrm{H_2O}} = 1.80$), respectively, and f_{Si} is the filling factor of Si-QDs, for the dielectric function of the shell.[33] By using the effective dielectric function, we calculate the extinction spectrum of the composite by extension of the Mie theory to a multilayered sphere.[34] The dielectric function of Au was approximated using a modified Drude model.[35] Figure 3b shows calculated extinction spectra for different shell thicknesses when f_{Si} is 0.045. The LSPR peak shifts from 530 to 547 nm with increasing thickness. In Figure 3c, the LSPR wavelength is plotted as a function of the shell thickness for different f_{Si} values. A larger f_{Si} results in a larger shift of the LSPR peak, because of the larger dielectric constant of Si than that of water. In Au-NP/Si-QD composites, the largest shift observed is about 10 nm, which suggests a relatively small value of f_{Si}. In the following calculation, we employ $f_{\mathrm{Si}} = 0.045$, in which case the observed peak shifts coincided with the calculation fairly well.

By using the effective dielectric function, we first calculate the enhancement factor of the electric field in the shell when a plane wave is incident by using extension of the Mie theory to a multilayer sphere.[34] Figure 3d shows a square of the

DOI: 10.1021/acs.jpcc.5b08105
J. Phys. Chem. C 2015, 119, 25108–25113

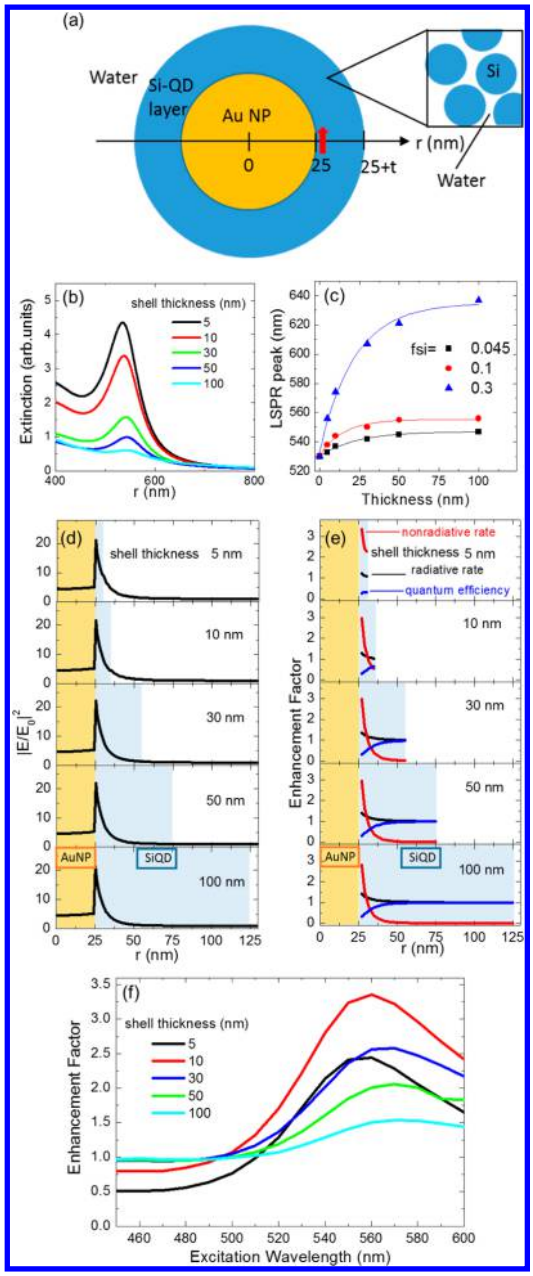

Figure 3. (a) Model structure for calculation of the PL enhancement factor of Au-NP/Si-QD composites. (b) Calculated extinction spectra for different shell thicknesses. f_{Si} is fixed to 0.045. (c) Peak wavelengths of calculated spectra for different f_{Si} values as a function of the shell thickness. (d) Enhancement factor of the square of the incident electric field as a function of the distance from the center of a Au-NP for different shell thicknesses. The wavelength is 550 nm. (e) Enhancement factor of radiative (P_{rad}) and nonradiative (P_{nrad}) decay rates and quantum efficiency of the optical antenna ($P_{rad}/(P_{rad} + P_{nrad})$). The emission wavelength is fixed at 780 nm. (f) PL enhancement factor at 780 nm as a function of the excitation wavelength for different shell thicknesses.

enhancement factor of the electric field along the radial direction for different shell thicknesses (5−100 nm). The electric field is averaged by integrating around a Au-NP in the circumferential direction. The enhancement factor is normalized by the square of the electric fields calculated for spherical Si-QD agglomerates with the same diameter and the same f_{Si}. The wavelength is 550 nm. In Figure 3d, the electric field is enhanced by at most 20-fold in the vicinity of Au-NPs. The enhancement factor is almost independent of the shell thickness. This is because the dielectric function of the shell is close to that of water due to the small f_{Si}.

As discussed above, the LSPR does not overlap with the PL band, and thus, the decay process is not expected to be modified by the LSPR. In fact, the PL decay rates do not change before and after the formation of composites (Figure 2e). However, even if the PL is off-resonance with the LSPR, the PL of Si-QDs very close to Au-NPs, where the enhancement of the incident electric field is the largest, is severely quenched due to absorption by interband transitions of Au-NPs.[31] To take into account the effect, we calculate the enhancement factors of radiative and nonradiative decay rates.[36] The radiative rate (P_{rad}) is calculated by integrating the time-averaged Poynting vector of a dipole in a shell over the surface of a sphere with an infinite radius. The nonradiative rate (P_{nrad}) is calculated by integrating the energy inflow per a unit time and a unit volume over the entire absorbing region. The calculated values are normalized by a calculated radiative decay rate of a Si-QD sphere with the same volume. Figure 3e shows the calculated results for different shell thicknesses. As expected, P_{rad} is almost 1 and independent of the distance and the shell thickness due to off-resonance. On the other hand, P_{nrad} of a dipole located in the vicinity of a Au-NP is very large and approaches 0 when the distance increases. In Figure 3e, $P_{rad}/(P_{rad} + P_{nrad})$, which is often called the quantum efficiency of the optical antenna, is also plotted.[37,38] Because of the large nonradiative rate, $P_{rad}/(P_{rad} + P_{nrad})$ is very small near a Au-NP and approaches 1 with increasing distance.

The enhancement factor of the PL intensity (EF) can be calculated by integrating the product of $|E/E_0|^2$ and $P_{rad}/(P_{rad} + P_{nrad})$ over the volume of the shells. Figure 3f shows calculated enhancement factors of the PL intensity as a function of the excitation wavelength for different shell thicknesses. For the calculation the emission wavelength is set to 780 nm. In all the thicknesses, PL enhancement near the LSPR wavelength can be seen. However, the enhancement factor depends on the shell thickness. When the shell thickness is 5 nm, the enhancement is relatively small due to the large P_{nrad} near Au-NPs. The enhancement factor increases until the thickness is 10 nm and then decreases. The decrease is due to the smaller incident field enhancement at larger distances. Note that the optimum thickness and the maximum enhancement factor depend also on the size of the Au-NPs, although in this work we fix the Au-NP diameter to 50 nm.

The calculated shell thickness dependence of the enhancement factor is in qualitatively agreement with the experimental results in Figure 2. Furthermore, the observed decrease of the PL intensity in the short wavelength range is reproduced in Figure 3f, when the shell thickness is small. The overall agreements between the experimental and calculated results indicate that the observed enhancement of the excitation efficiency is due to coupling of Si-QDs with the LSPR of Au-NPs and the formation of composites is a promising approach to enhance the excitation efficiency of Si-QDs.

■ CONCLUSION

We have developed a composite NP consisting of a Au-NP and a thick layer of Si-QDs covering the Au-NP and demonstrated that the excitation efficiency of the PL from Si-QDs is enhanced in the LSPR wavelength range by the composite formation. The observed enhancement could be well-explained by a model

DOI: 10.1021/acs.jpcc.5b08105
J. Phys. Chem. C 2015, 119, 25108−25113

assuming a Au-NP core and a spherical shell of Si-QDs. The calculation revealed that the enhancement is due to the increased excitation efficiency of Si-QDs via the LSPR of Au-NPs. The excitation efficiency enhancement in a long wavelength range enables higher sensitivity and deeper imaging of biological substances in Si-QD-based materials.

■ ASSOCIATED CONTENT

Supporting Information

The Supporting Information is available free of charge on the ACS Publications website at DOI: 10.1021/acs.jpcc.5b08105.

TEM images of composite NPs and PL spectra of Si-QDs and Au-NP/Si-QD composites (PDF)

■ AUTHOR INFORMATION

Corresponding Author

*E-mail: fujii@eedept.kobe-u.ac.jp.

Notes

The authors declare no competing financial interest.

■ ACKNOWLEDGMENTS

H.S. acknowledges a Grant-in-Aid for Japan Society for the Promotion of Science (JSPS) Fellows (Grant 26-3120). This work was supported by the 2014 JSPS Bilateral Joint Research Projects (Japan−Czech Republic).

■ REFERENCES

(1) Gao, X.; Cui, Y.; Levenson, R. M.; Chung, L. W. K.; Nie, S. In Vivo Cancer Targeting and Imaging with Semiconductor Quantum Dots. *Nat. Biotechnol.* **2004**, *22*, 969−976.

(2) Michalet, X. Quantum Dots for Live Cells, in Vivo Imaging, and Diagnostics. *Science* **2005**, *307*, 538−544.

(3) Chan, W. C. W.; Maxwell, D. J.; Gao, X.; Bailey, R. E.; Han, M.; Nie, S. Luminescent Quantum Dots for Multiplexed Biological Detection and Imaging. *Curr. Opin. Biotechnol.* **2002**, *13*, 40−46.

(4) Resch-Genger, U.; Grabolle, M.; Cavaliere-Jaricot, S.; Nitschke, R.; Nann, T. Quantum Dots versus Organic Dyes as Fluorescent Labels. *Nat. Methods* **2008**, *5*, 763−775.

(5) Tsoi, K. M.; Dai, Q.; Alman, B. A.; Chan, W. C. W. Quantum Dots Toxic? Exploring the Discrepancy Between Cell Culture and Animal Studies. *Acc. Chem. Res.* **2013**, *46*, 662−671.

(6) Fujioka, K.; Hiruoka, M.; Sato, K.; Manabe, N.; Miyasaka, R.; Hanada, S.; Hoshino, A.; Tilley, R. D.; Manome, Y.; Hirakuri, K.; et al. Luminescent Passive-Oxidized Silicon Quantum Dots as Biological Staining Labels and Their Cytotoxicity Effects at High Concentration. *Nanotechnology* **2008**, *19*, 415102.

(7) Erogbogbo, F.; Tien, C. A.; Chang, C. W.; Yong, K. T.; Law, W. C.; Ding, H.; Roy, I.; Swihart, M. T.; Prasad, P. N. Bioconjugation of Luminescent Silicon Quantum Dots for Selective Uptake by Cancer Cells. *Bioconjugate Chem.* **2011**, *22*, 1081−1088.

(8) Erogbogbo, F.; Yong, K. T.; Roy, I.; Xu, G. X.; Prasad, P. N.; Swihart, M. T. Biocompatible Luminescent Silicon Quantum Dots for Imaging of Cancer Cells. *ACS Nano* **2008**, *2*, 873−878.

(9) Mcvey, B. F. P.; Tilley, R. D. Solution Synthesis, Optical Properties, and Bioimaging Applications of Silicon Nanocrystals. *Acc. Chem. Res.* **2014**, *47*, 3045−3051.

(10) Li, Z. F.; Ruckenstein, E. Water-Soluble Poly(acrylic Acid) Grafted Luminescent Silicon Nanoparticles and Their Use as Fluorescent Biological Staining Labels. *Nano Lett.* **2004**, *4*, 1463−1467.

(11) O'Farrell, N. O.; Houlton, A.; Horrocks, B. R. Silicon Nanoparticles: Applications in Cell Biology and Medicine. *Int. J. Nanomed.* **2006**, *1*, 451−472.

(12) Montalti, M.; Cantelli, A.; Battistelli, G. Nanodiamonds and Silicon Quantum Dots: Ultrastable and Biocompatible Luminescent Nanoprobes for Long-Term Bioimaging. *Chem. Soc. Rev.* **2015**, *44*, 4853−4921.

(13) Park, J.-H.; Gu, L.; von Maltzahn, G.; Ruoslahti, E.; Bhatia, S. N.; Sailor, M. J. Biodegradable Luminescent Porous Silicon Nanoparticles for in Vivo Applications. *Nat. Mater.* **2009**, *8*, 331−336.

(14) He, Y.; Kang, Z.-H.; Li, Q.-S.; Tsang, C. H. A.; Fan, C.-H.; Lee, S.-T. Ultrastable, Highly Fluorescent, and Water-Dispersed Silicon-Based Nanospheres as Cellular Probes. *Angew. Chem.* **2009**, *121*, 134−138.

(15) Weissleder, R. A Clearer Vision for in Vivo Imaging. *Nat. Biotechnol.* **2001**, *19*, 316−317.

(16) Sugimoto, H.; Fujii, M.; Imakita, K.; Hayashi, S.; Akamatsu, K. Codoping N- and P-Type Impurities in Colloidal Silicon Nanocrystals: Controlling Luminescence Energy from below Bulk Band Gap to Visible Range. *J. Phys. Chem. C* **2013**, *117*, 11850−11857.

(17) Mastronardi, M. L.; Maier-Flaig, F.; Faulkner, D.; Henderson, E. J.; Kübel, C.; Lemmer, U.; Ozin, G. A. Size-Dependent Absolute Quantum Yields for Size-Separated Colloidally-Stable Silicon Nanocrystals. *Nano Lett.* **2012**, *12*, 337−342.

(18) Mertens, H.; Biteen, J. S.; Atwater, H. A.; Polman, A. Polarization-Selective Plasmon-Enhanced Silicon Quantum-Dot Luminescence. *Nano Lett.* **2006**, *6*, 2622−2625.

(19) Biteen, J. S.; Pacifici, D.; Lewis, N. S.; Atwater, H. A. Enhanced Radiative Emission Rate and Quantum Efficiency in Coupled Silicon Nanocrystal-Nanostructured Gold Emitters. *Nano Lett.* **2005**, *5*, 1768−1773.

(20) Mochizuki, Y.; Fujii, M.; Hayashi, S.; Tsuruoka, T.; Akamatsu, K. Enhancement of Photoluminescence from Silicon Nanocrystals by Metal Nanostructures Made by Nanosphere Lithography. *J. Appl. Phys.* **2009**, *106*, 013517.

(21) Wang, Y.; Sugimoto, H.; Inampudi, S.; Capretti, A.; Fujii, M.; Dal Negro, L. Broadband Enhancement of Local Density of States Using Silicon-Compatible Hyperbolic Metamaterials. *Appl. Phys. Lett.* **2015**, *106*, 241105.

(22) Sugimoto, H.; Zhang, R.; Reinhard, B. M.; Fujii, M.; Perotto, G.; Marelli, B.; Omenetto, F. G.; Dal Negro, L. Enhanced Photoluminescence of Si Nanocrystals-Doped Cellulose Nanofibers by Plasmonic Light Scattering. *Appl. Phys. Lett.* **2015**, *107*, 041111.

(23) Erogbogbo, F.; Liu, X.; May, J. L.; Narain, A.; Gladding, P.; Swihart, M. T.; Prasad, P. N. Plasmonic Gold and Luminescent Silicon Nanoplatforms for Multimode Imaging of Cancer Cells. *Integr. Biol.* **2013**, *5*, 144−150.

(24) Harun, N. A.; Benning, M. J.; Horrocks, B. R.; Fulton, D. a. Gold Nanoparticle-Enhanced Luminescence of Silicon Quantum Dots Co-Encapsulated in Polymer Nanoparticles. *Nanoscale* **2013**, *5*, 3817−3827.

(25) Sugimoto, H.; Chen, T.; Wang, R.; Fujii, M.; Reinhard, B. M.; Dal Negro, L. Plasmon-Enhanced Emission Rate of Silicon Nanocrystals in Gold Nanorod Composites. *ACS Photonics* **2015**, *2*, 1298−1305.

(26) Sugimoto, H.; Fujii, M.; Imakita, K.; Hayashi, S.; Akamatsu, K. All-Inorganic near-Infrared Luminescent Colloidal Silicon Nanocrystals: High Dispersibility in Polar Liquid by Phosphorus and Boron Codoping. *J. Phys. Chem. C* **2012**, *116*, 17969−17974.

(27) Sugimoto, H.; Fujii, M.; Fukuda, Y.; Imakita, K.; Akamatsu, K. All-Inorganic Water-Dispersible Silicon Quantum Dots: Highly Efficient near-Infrared Luminescence in a Wide pH Range. *Nanoscale* **2014**, *6*, 122−126.

(28) Sugimoto, H.; Fujii, M.; Imakita, K.; Hayashi, S.; Akamatsu, K. Phosphorus and Boron Codoped Colloidal Silicon Nanocrystals with Inorganic Atomic Ligands. *J. Phys. Chem. C* **2013**, *117*, 6807−6813.

(29) Fujii, M.; Sugimoto, H.; Hasegawa, M.; Imakita, K. Silicon Nanocrystals with High Boron and Phosphorus Concentration Hydrophilic shell—Raman Scattering and X-Ray Photoelectron Spectroscopic Studies. *J. Appl. Phys.* **2014**, *115*, 084301.

(30) Schneider, G.; Decher, G. From Functional Core/Shell Nanoparticles Prepared via Layer-by-Layer Deposition to Empty Nanospheres. *Nano Lett.* **2004**, *4*, 1833−1839.

DOI: 10.1021/acs.jpcc.5b08105
J. Phys. Chem. C 2015, 119, 25108−25113

(31) Jain, P. K.; El-Sayed, M. A. Plasmonic Coupling in Noble Metal Nanostructures. *Chem. Phys. Lett.* **2010**, *487*, 153−164.
(32) Palik, E. D. *Handbook of Optical Constants of Solids*; Academic Press: San Diego, CA, 1998; Vol. 3.
(33) Bruggeman, D. A. G. Calculation of Various Physics Constants in Heterogenous Substances I Dielectricity Constants and Conductivity of Mixed Bodies from Isotropic Substances. *Ann. Phys.* **1935**, *416*, 665−679.
(34) Johnson, B. R. Light Scattering by a Multilayer Sphere. *Appl. Opt.* **1996**, *35*, 3286−3296.
(35) Johnson, P. B.; Christy, R. W. Optical Constants of the Noble Metals. *Phys. Rev. B* **1972**, *6*, 4370−4379.
(36) Moroz, A. A Recursive Transfer-Matrix Solution for a Dipole Radiating Inside and Outside a Stratified Sphere. *Ann. Phys. (Amsterdam, Neth.)* **2005**, *315*, 352−418.
(37) Wang, W.; He, D.; Duan, J.; Fu, M.; Zhang, X.; Wu, H.; Hu, Y.; Wang, Y. Modulated Photoluminescence of Graphene Quantum Dots in the Vicinity of an Individual Silver Nano-Octahedron. *Phys. Chem. Chem. Phys.* **2014**, *16*, 4504−4509.
(38) Novotny, L.; van Hulst, N. Antennas for Light. *Nat. Photonics* **2011**, *5*, 83−90.

DOI: 10.1021/acs.jpcc.5b08105
J. Phys. Chem. C 2015, 119, 25108−25113